

Phase Equilibria of $\text{SiO}_2\text{-Ce}_2\text{O}_3\text{-CaO-25wt.}\%$ Al_2O_3 System at 1773 K



Rensheng Li, Mengchuan Li, Tongsheng Zhang, and Wanlin Wang

Abstract The utilization of rare earth resources, especially secondary resources (e.g., RE-oxide system slag), has been limited by the lack of thermodynamic information. In order to supplement and refine the thermodynamic data related to rare earth, the equilibrium experiments of $\text{SiO}_2\text{-Ce}_2\text{O}_3\text{-CaO-25wt.}\%$ Al_2O_3 system phase diagram were carried out at 1773 K by the high-temperature isothermal equilibration/quenching technique in the current paper. The composition of seven phase regions was determined by FE-SEM, XRD, EPMA, and XRF analysis on the samples obtained by high-temperature equilibrium technology at 1773 K, including the primary crystal regions of three compounds (C_2AS , $2\text{CaO}\cdot\text{SiO}_2$, and $\text{CaO}\cdot 2\text{Ce}_2\text{O}_3\cdot 3\text{SiO}_2$), three three-phase coexistence regions ($\text{L} + \text{C}_2\text{AS} + 2\text{CaO}\cdot\text{SiO}_2$, $\text{L} + \text{C}_2\text{AS} + \text{CaO}\cdot 2\text{Ce}_2\text{O}_3\cdot 3\text{SiO}_2$, and $\text{L} + \text{CaO}\cdot 2\text{Ce}_2\text{O}_3\cdot 3\text{SiO}_2 + \text{CeAl}_{11}\text{O}_{18}$), and a liquid region. The phase relations and isotherms of $\text{SiO}_2\text{-Ce}_2\text{O}_3\text{-CaO-25wt.}\%$ Al_2O_3 system obtained in current work are beneficial to the recycling of rare earth resources containing cerium.

Keywords Rare earth · Phase equilibria · Experimental thermodynamics · Liquidus

R. Li · M. Li
School of Metallurgy and Environment, Central South University,
Changsha 410083, P. R. China
e-mail: rensheng_li@163.com

M. Li
e-mail: csu_lmc@163.com

T. Zhang (✉) · W. Wang
School of Metallurgy and Environment, Central South University, Changsha 410083, P. R. China
e-mail: tongsheng.zhang@csu.edu.cn

Introduction

Generally speaking, the research methods of phase diagram include theoretical calculation and experimental determination. Theoretical calculation refers to the thermodynamic database based on strict thermodynamic data, so as to accurately describe a specific system. Therefore, to ensure the accuracy of the calculated phase diagram, a large number of reliable experimental data are necessary to determine the parameters in the thermodynamic model. So, determining the phase of some systems with practical application value through experiments is necessary.

Lanthanide elements from La to Lu as well as Y and Sc are collectively referred to as rare earth elements (REEs) due to their similar chemical properties [1]. REEs have high chemical activity and play a significant role in many new materials fields. In particular, the improvement of mechanical properties of ceramic materials and steel materials by REEs has attracted more and more attention [2]. In recent years, with the global consumption of high-grade rare earth resources increasing significantly, the recycling of waste containing rare earth has been brought into focus [3].

As we all know, the Bayan Obo deposit in Inner Mongolia, North China is rich in rare earth, titanium, iron, fluoride, and other precious resources [4]. However, the associated beneficiation and smelting processes are very hard because it is a typical polymetallic ore, and valuable components coexist [5, 6]. Besides, due to the limitations of current technologies, the utilization rate of rare earth resources is very low. Only about 10% of the rare earth resources in the world are utilized, which is out of proportion to their value [7]. More importantly, with the accumulation of tailings dams, many serious environmental problems such as water pollution have emerged. Therefore, the effective recovery and application of rare earth elements are of great significance to the sustainable utilization of rare earth slag [8].

Recently, many scholars have studied and reported a great number of phase equilibrium data of binary and ternary systems in rare earth slag systems. Tas et al. [9] studied $\text{Al}_2\text{O}_3\text{-Ce}_2\text{O}_3$ system, and found that there are two binary compounds ($\text{CeAl}_{11}\text{O}_{18}$ and CeAlO_3) in the system, and provided lattice constants of $\text{CeAl}_{11}\text{O}_{18}$. At 1873 K, two solid solution phases ($\text{Ce}_{9.33-x}\text{Ca}_x(\text{SiO}_2)_6\text{O}_{2-8}$ and $\text{Ca}_{2-x}\text{Ce}_x\text{SiO}_{4+\delta}$) were found in $\text{SiO}_2\text{-Ce}_2\text{O}_3\text{-CaO}$ system, and the formulae for calculating the activity of Ce_2O_3 are provided [10]. Lan et al. [11, 12] provided the phase diagrams of $\text{SiO}_2\text{-Ce}_2\text{O}_3\text{-CaO}$ system at 1573 and 1773 K, and the phase diagrams of $\text{CaO-SiO}_2\text{-CaF}_2\text{-Ce}_2\text{O}_3$ system at 1373 K. As we all know, P and F are also the main compositions in rare earth ores, and they are transferred to the slag containing rare earth, which affects the composition and performance of the slag. Therefore, Lan constructed an isothermal pseudo-ternary phase diagram of $\text{CaO-SiO}_2\text{-CaF}_2$ (30wt. %)- P_2O_5 (10wt. %)- Ce_2O_3 and obtained the formation mechanism of boro-magnesium olivine in the five-member system [13].

Recently, many different phases of REEs have been found in slag containing rare earth elements in previous studies. By analyzing and simulating the morphology of slag containing rare earth elements, Li et al. [14] found that rare earth elements are converted into calcium-cerite phase. Ding et al. [15] reported that rare earth

elements mainly exist in the form of cephalosilicate in the rare earth slag produced from Bayan Obo ore. Therefore, the supplement and improvement of thermodynamic information can also help researchers to confirm that the rare earth phase is a series of component transformation behaviors according to the formation and transformation information of rare earth phase in equilibrium state. On this basis, the equilibrium phase composition of SiO₂-Ce₂O₃-CaO-25wt.% Al₂O₃ at 1773 K was studied in this paper, which provides basic phase transition data for the recycling of rare earth waste residue in ceramics and other fields.

Methodology

Rare Earth Slag Samples Preparation

Generally speaking, isothermal pseudo-ternary phase diagrams can be constructed by fixing typical components, so as to simplify the study of phase equilibrium in multicomponent systems. In order to obtain uniform composition and ensure the accuracy of the experiment, firstly, the SiO₂, CaO, CeO₂, and Al₂O₃ powders of 99.99% purity (Sinopharm Chemical Reagents Co., Ltd.) were put into a muffle furnace and calcined at 1273 K for 6 h to remove moisture and impurities. The raw materials were accurately weighed by an electronic balance with an accuracy of 0.0001 g, and then used to make slags. Every slag was then ground by an agate mortar for 30 min, so that it can be fully and uniformly mixed. Thereafter, the pre-mixed slags were put into a vertical furnace (temperature measurement accuracy ± 1 K) with Ar + 10% H₂ atmosphere. The powdered slags in platinum crucibles were heated to 1923 K for 2 h. Then, the molten samples were quickly quenched in the ice-water mixture. In current study, it is a key point to ensure the complete transformation of CeO₂ into Ce₂O₃. Therefore, we referred to a large number of literatures [9–13] and adopted the same reduce atmosphere. The oxygen partial pressure was controlled below 2×10^{-16} during the experiment process. Based on these experimental conditions, we also conducted X-ray Photoelectron Spectroscopy (XPS) test on all of the samples. Taking sample N1 for example, the 3d_{5/2} and 3d_{3/2} XPS lines of the Ce³⁺ ion is presented in Fig. 1. Because of the transition behavior between different energy levels of Ce³⁺ ion, the 3d_{5/2} doublet and the 3d_{3/2} doublet appear [16, 17]. The results showed that only Ce³⁺ but no Ce⁴⁺ existed in the pre-melting samples.

X-ray diffraction (XRD, D/max 2550VB) detection is required for all slag samples to ensure the uniform glass phase after quenching. If crystal precipitation was detected in the sample, the sample would be reproduced for the supplementary experiment. The content of each oxide will be readjusted, and the slag samples pre-melting test will be conducted again until all the required quenched samples completely show the glass phase. Figure 2 shows the microstructure (a) and XRD patterns (b) of the glass phase sample N1.

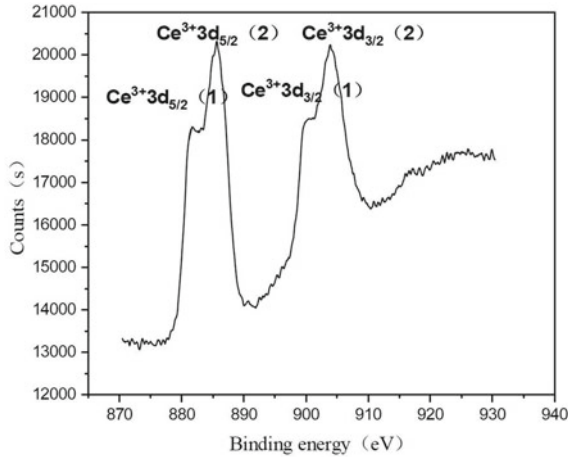


Fig. 1 XPS detection map of quenching slag sample N1

Because of burning loss and batching error, the composition of quenching slags may be different from that of samples, so it was necessary to detect the composition of quenching slags to determine the composition of slag samples again to ensure the accuracy of the experiment. X-Ray Fluorescence Spectrometer (XRF, Axios mAX) was used to analyze the composition of quenching slag samples, and the results are listed in the pseudo ternary phase diagram of $\text{SiO}_2\text{-Ce}_2\text{O}_3\text{-CaO-25wt. \% Al}_2\text{O}_3$ system, as shown in Fig. 3.

Equilibration Experiments

In the equilibration experiments, a box furnace, as shown in Fig. 4a, was used, and the temperature was detected by a B-type thermocouple placed at the bottom of the furnace. The overall temperature accuracy is ± 1 K. High-purity argon with 10% hydrogen, purified by gas purification unit as shown in Fig. 4b, was continuously inject as protective gas to avoid the oxidation of slag samples and isolated other possible pollution sources. The deoxidation unit consists of a heating device, and a deoxidation chamber with copper, sponge titanium, and magnesium, which can keep the partial pressure of oxygen in argon gas below 10^{-16} . About 2 g of homogenized glass-phase slag sample was loaded into a platinum crucible and placed in the constant temperature zone of the box furnace. All samples were heated to 1923 K again and held for 30 min, then cooled to the target equilibrium temperature (1773 K) at a rapid rate (10 K/min). Based on preliminary experimental results and previous experimental experience [18], the time was set at 24 h to ensure that the equilibrium is achieved.

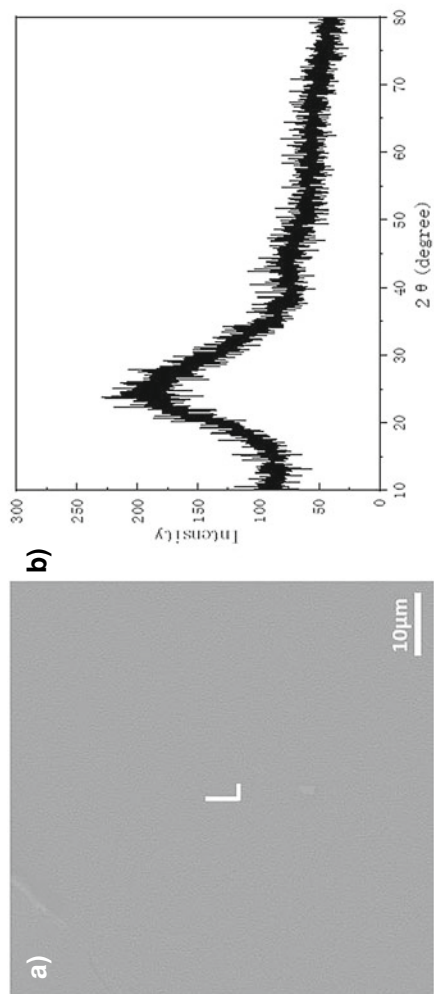


Fig. 2 Microstructure (a) and XRD patterns (b) of pre-melted slag sample N1

Fig. 3 Pre-melting component points of $\text{SiO}_2\text{-Ce}_2\text{O}_3\text{-CaO-25wt. \% Al}_2\text{O}_3$ system at 1773 K

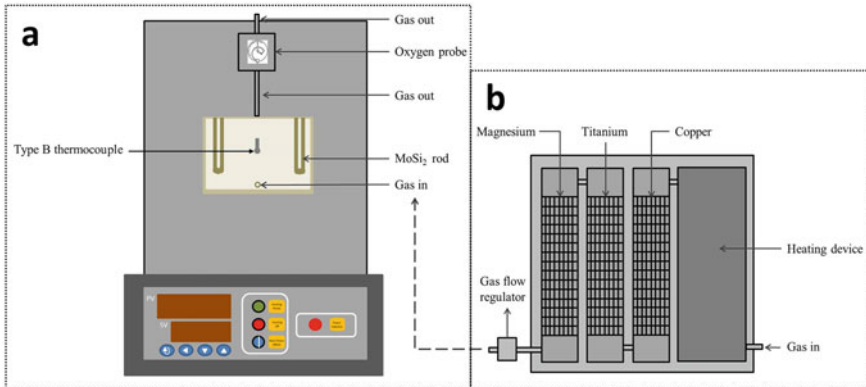
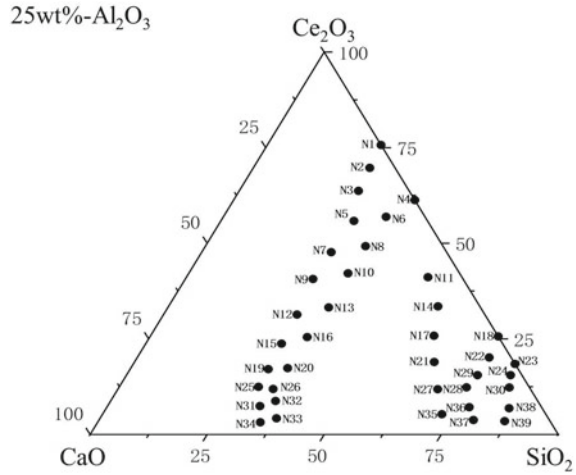


Fig. 4 Schematic diagram of box-type furnace (a) and gas purification unit (b)

When the samples reached equilibrium, they were rapidly quenched into the ice-water mixture. Then the quenched slag samples were dried at room temperature. Electron probe microanalysis (EPMA, JXA-8230) was used to analyze the composition of each sample, and the precipitated phase contained in hardened slag samples was detected by XRD. In addition, scanning electron microscope (SEM, JSM-7900F) was used to observe the coexisting phase. The equilibrium micro-morphology of the samples was obtained in BSE mode. SEM test conditions are: beam current 15 mA, electron beam acceleration voltage 20 kV. The EPMA measurement conditions were as follows: a beam current of 10^{-8} A, an accelerating potential of 20 kV, and a probe diameter of 1 μm . CaSiO_3 , Al_2O_3 , and $\text{CeP}_5\text{O}_{14}$ were respectively used as standards

to analyze CaO and SiO₂, Al₂O₃, Ce₂O₃. For each balancing stage, more than 10 different points were analyzed and average values were calculated. Combining the results of XRD, FE-SEM, and EPMA, the phase composition of those samples in equilibrium state was obtained.

Results and Discussion

Equilibrium Phase Composition of SiO₂-Ce₂O₃-CaO-25wt.% Al₂O₃ System at 1773 K

In general, by fixing typical components to construct isothermal pseudo-ternary phase diagram, the investigation related to the multicomponent system phase equilibrium can be simplified [19]. When quenched to room temperature, some samples would have a large amount of secondary precipitation, which leads to inaccurate liquidus composition and is an important reason for the failure of the experiment. Therefore, some samples were selected to study the phase equilibrium of SiO₂-Ce₂O₃-CaO-25wt.% Al₂O₃ system. The results of FE-SEM and XRD show that the quenched samples consist of amorphous glass and crystalline phase. The crystalline phase is precipitated from the solid phase at 1773 K, while the glassy phase is formed by quenching and supercooling the liquid phase in equilibrium with the solid phase.

The results of EPMA and XRD, which measured the chemical composition of glass phase and crystal phase, show that there are seven different equilibrium phases. Those seven equilibrium phases in order are: (1) the simple liquid phase; (2) the three-phase equilibrium between C₂AS (2CaO·Al₂O₃·SiO₂), 2CaO·SiO₂, and liquid phase; (3) the solid–liquid coexistence of C₂AS and liquid phase; (4) the three-phase equilibrium between C₂AS, CaO·2Ce₂O₃·3SiO₂, and liquid phase; (5) the solid–liquid coexistence of CaO·2Ce₂O₃·3SiO₂ and liquid phase; (6) the three-phase equilibrium between CaO·2Ce₂O₃·3SiO₂, CeAl₁₁O₁₈ and liquid phase; (7) the solid–liquid coexistence of 3Al₂O₃·2SiO₂ and liquid phase. Due to the replacement mechanism of Ca and REEs, Ce³⁺ will replace a part of Ca²⁺, which cause that about 3–5wt% of CaO are replaced by REEs in the sorosilicate phase [20]. Therefore, it is remarkable that Ce³⁺ can replace part of Ca²⁺ in the compounds Ca₂SiO₄ and C₂AS, resulting in (Ca,Ce)₂SiO₄ and 2(Ca,Ce)O·Al₂O₃·SiO₂. Gao [21] found the solid solution CaO·2Ce₂O₃·3SiO₂ during the reduction process, whose research results are the same as these in current study. The microstructure and composition of the equilibrium phase at 1773 K are shown in Fig. 5 and Table 1, respectively. As is known to all, the liquid phase area gradually expands as the temperature increases.

The phase structure of sample N33 at 1773 K is shown in Fig. 5a, showing three-phase coexistence. Combined with the detection results of EPMA and XRD, it can be found that the dark gray region is calcium aluminite melilite phase

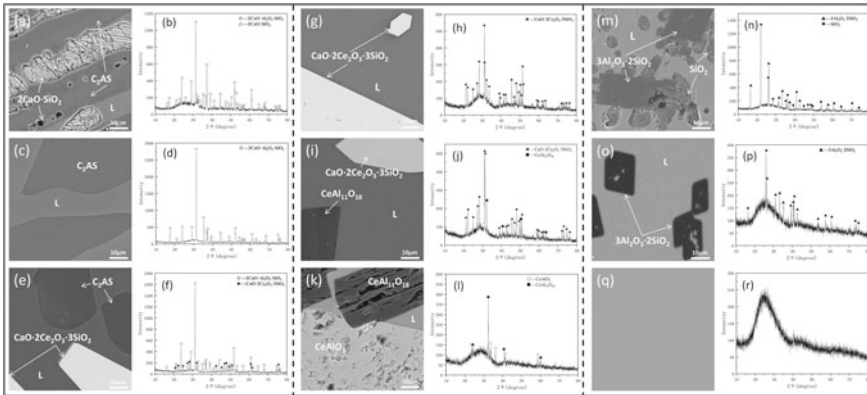


Fig. 5 Microstructure of equilibrium phase of SiO₂-Ce₂O₃-CaO-25wt. % Al₂O₃ system at 1773 K and corresponding XRD detection patterns. **a, c, e, g, i, k, m, o,** and **q** represent the Micromorphology of N33, N26, N9, N3, N2, N1, N18, N24, and N11 sample, respectively; and **b, d, f, h, j, l, n, p,** and **r** were XRD patterns of corresponding sample

(2CaO·Al₂O₃·SiO₂, C₂AS), the gray region is quenched liquid phase, and the light gray region is Mosaic (2CaO·SiO₂). For samples N32 and N34, the same precipitated phase, calcium aluminite melilite phase, appears, as shown in Fig. 5c. According to EPMA and XRD results, the gray region is the quenching liquid phase.

The microstructure of sample N9 is shown in Fig. 5e. According to the BSE picture, it can be clearly found that the equilibrium phase presents a state of three-phase coexistence. According to EPMA and XRD results, it can be easily confirmed that the dark gray region is still C₂AS, and the gray region is quenched liquid phase. The most recent white region can be identified as CaO·2Ce₂O₃·3SiO₂ phase. In addition, CaO·2Ce₂O₃·3SiO₂ phase also exists in samples N3, N5, and N10. Their microstructures are shown in Fig. 5g and 5(i). At 1773 K, there are only two equilibrium phases CaO·2Ce₂O₃·3SiO₂ phase and quenched liquid phase in samples N5 and N10. The results indicate that the composition of slag sample N5 and slag sample N10 is in the primary crystal region of CaO·2Ce₂O₃·3SiO₂, and there are grey CaO·2Ce₂O₃·3SiO₂ phase and light gray quenching liquid phase in sample N2, as well as dark gray long CeAl₁₁O₁₈ phase. For sample N1, the microstructure is shown in Fig. 5k, and the CeAl₁₁O₁₈ phase shows a black band. The white area can be identified as CeAlO₃ phase according to the XRD and EPMA detection results.

Table 1 Equilibrium phase compositions at 1773 K

Sample No	Phase	Composition (wt%)			
		Al ₂ O ₃	SiO ₂	Ce ₂ O ₃	CaO
N1	L	25.25	26.13	48.62	0
	CeAl ₁₁ O ₁₈	82.1	0.62	16.85	0.43
	CeAlO ₃	32.72	0.43	66.43	0.42
N2	L	27.46	29.25	39.21	4.08
	CeAl ₁₁ O ₁₈	82.18	0.89	16.28	0.65
	CaO·2Ce ₂ O ₃ ·3SiO ₂	1.59	22.27	69.57	6.57
N3	L	28.26	27.90	32.68	11.16
	CeAl ₁₁ O ₁₈	82.26	0.48	16.76	0.5
	CaO·2Ce ₂ O ₃ ·3SiO ₂	1.29	22.08	70.16	6.47
N5	L	30.49	27.41	26.17	15.92
	CaO·2Ce ₂ O ₃ ·3SiO ₂	1.14	22.12	70.19	6.55
N7*	L	32.18	25.11	21.32	21.39
	C ₂ AS	37.13	21.1	5.93	35.84
	CaO·2Ce ₂ O ₃ ·3SiO ₂	1.32	22.13	70.16	6.39
N9*	L	31.83	25.88	20.98	21.31
	C ₂ AS	37.09	20.58	5.95	36.38
	CaO·2Ce ₂ O ₃ ·3SiO ₂	1.65	21.8	68.94	7.61
N10	L	32.37	26.69	22.09	18.85
	CaO·2Ce ₂ O ₃ ·3SiO ₂	1.08	22.59	68.93	7.4
N12*	L	22.44	32.18	16.12	29.26
	C ₂ AS	36.9	22.11	5.13	35.86
	CaO·2Ce ₂ O ₃ ·3SiO ₂	1.2	21.42	70.31	7.07
N13*	L	28.93	29.32	18.14	23.61
	C ₂ AS	38.28	20.12	4.43	37.17
	CaO·2Ce ₂ O ₃ ·3SiO ₂	0.98	21.08	70.99	6.95
N16*	L	24.37	32.45	15.90	27.28
	C ₂ AS	38.63	20.89	3.87	36.61
	CaO·2Ce ₂ O ₃ ·3SiO ₂	1.41	20.82	70.75	7.02
N20*	L	19.79	33.77	14.85	31.59
	C ₂ AS	37.55	22.24	3.15	37.06
	CaO·2Ce ₂ O ₃ ·3SiO ₂	0.87	21.67	70.52	6.94
N23	L	20.78	52.61	26.61	0
	3Al ₂ O ₃ ·2SiO ₂	70.83	25.83	2.42	0.92

(continued)

Table 1 (continued)

Sample No	Phase	Composition (wt%)			
		Al ₂ O ₃	SiO ₂	Ce ₂ O ₃	CaO
	SiO ₂	0.02	99.68	0.14	0.16
N24	L	18.03	64.56	11.85	5.56
	3Al ₂ O ₃ ·2SiO ₂	71.43	25.13	2.61	0.83
N26*	L	13.50	34.57	14.43	37.50
	C ₂ AS	37.86	20.57	3.93	37.64
	CaO·2Ce ₂ O ₃ ·3SiO ₂	0.22	22.9	69.71	7.17
N30	L	21.87	57.71	16.89	3.53
	3Al ₂ O ₃ ·2SiO ₂	71.41	25.34	2.4	0.85
N32*	L	14.29	35.84	10.88	38.99
	C ₂ AS	38.32	21.65	4.42	35.61
N33*	L	12.72	35.51	3.75	48.02
	C ₂ AS	38.94	20.63	3.8	36.63
	2CaO·SiO ₂	1.54	32.23	6.14	60.09
N34*	L	15.38	36.58	6.78	41.26
	C ₂ AS	38.39	19.76	6.69	35.16
N38	L	21.05	64.84	6.80	7.31
	3Al ₂ O ₃ ·2SiO ₂	71.65	25.22	2.6	0.53
N39	L	21.99	64.65	3.74	9.62
	3Al ₂ O ₃ ·2SiO ₂	72.17	24.93	2.38	0.52

*represents the results obtained by converting Ce³⁺ into Ca²⁺

The microstructure of the equilibrium phase of sample N18 is shown in Fig. 5m. According to the results of EPMA and XRD, it can be known that the round, oval, and conical phase is SiO₂ phase, while the regular quadrilateral phase is 3Al₂O₃·2SiO₂ phase. Similarly, in the samples N24 and N30, the relatively regular quadrilateral 3Al₂O₃·2SiO₂ phase is detected, but their equilibrium phase structure only contained 3Al₂O₃·2SiO₂ phase and quenching liquid phase. Samples N11, N14, N17, N21, and N27 only contain quenched liquid phase, and it can be determined that there is no other precipitated phase according to the XRD detection results. Figure 5q and 5(r) are the microscopic morphology images and XRD detection patterns of quenched slag sample N14. It is worth noting that in the SiO₂-Ce₂O₃-CaO-5wt.% Al₂O₃ system previously studied [18], the initial crystal region of SiO₂ appears when the content of SiO₂ is higher than 70wt%. However, in this system, when the content of Al₂O₃ is increased from a fixed 5wt% to 25wt%, no initial crystal region of SiO₂ is found.

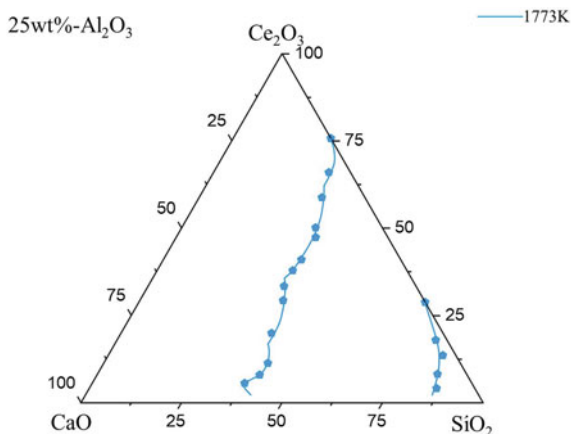
Table 1 lists the composition and content of liquid phase and precipitates of each sample. It should be noted that part of Ca²⁺ was replaced by Ce³⁺ in the sample with ‘*’. Thus, the precipitated phase Ca₂SiO₄ and C₂AS were obtained by converting Ce³⁺ into Ca²⁺.

Determination of the Isotherms

The composition of the quenched liquid phase was standardized so that the phase relationship of SiO₂-Ce₂O₃-CaO-25wt.% Al₂O₃ system can be represented by phase diagram [22, 23]. As shown in Fig. 6, the liquid phase isotherms of SiO₂-Ce₂O₃-CaO-25wt.% Al₂O₃ system at 1773 K are obtained based on the above experimental results.

As can be seen from the Fig. 6, the liquid phase region is concentrated in the SiO₂ content between about 38% and 75%. Meanwhile, with the increase of CaO content, the distance between the liquid phase isotherms of 1773 K is closer and closer, indicating that when the ratio of SiO₂ and Ce₂O₃ content is constant, the melting point of the mixture can be significantly increased by increasing the content of CaO in the mixture. And when the binary basicity (CaO/SiO₂) is certain, reducing the content of Ce₂O₃ can also achieve the effect of reducing the melting point of the mixture. Meanwhile, with the decrease of Ce₂O₃ content, the liquid phase region becomes larger. In the previous work [18], we studied the SiO₂-Ce₂O₃-CaO-5wt.% Al₂O₃ system and not found a liquid phase region at 1773 K at the phase boundary of SiO₂ and Ce₂O₃. While in this study, there was a large liquid phase region at the phase boundary of SiO₂ and Ce₂O₃ [18]. Therefore, we can speculate that in the ternary system of SiO₂-Ce₂O₃-Al₂O₃, there is a large liquid region at 1773 K with the increase of Al₂O₃.

Fig. 6 Liquid phase isotherms of SiO₂-Ce₂O₃-CaO-25wt.% Al₂O₃ system at 1773 K

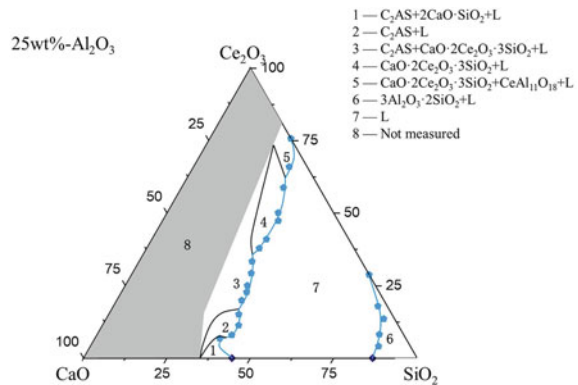


Construction of $\text{SiO}_2\text{-Ce}_2\text{O}_3\text{-CaO-25wt.\% Al}_2\text{O}_3$ System Phase Diagram

Phase diagram can be used to quantitatively describe the phase equilibrium of systems. It can help to determine the direction of a reaction and avoid the resource consumption during the research process. Combining the isotherms of $\text{SiO}_2\text{-Ce}_2\text{O}_3\text{-CaO-25wt.\% Al}_2\text{O}_3$ system at 1773 K with the above equilibrium phase structure, a phase diagram related to the system containing rare earth was constructed, as shown in Fig. 7. In Fig. 7, according to the trend of phase boundary, the intersection point of phase boundary is found. Meanwhile, several points on the CaO-SiO_2 phase boundary are data points obtained according to the known phase diagram [24].

In this study, there are six regions where equilibrium phase and liquid phase coexist, among which there are three single-phase regions, the primary phases are mullite phase, $\text{CaO}\cdot 2\text{Ce}_2\text{O}_3\cdot 3\text{SiO}_2$ phase, and calcium anorthite solid solution phase, and the other three are three-phase coexistence regions. From the equilibrium phase detected in 1773 K equilibrium slag samples, it can be seen that when SiO_2 content is higher than 75%, there is only $3\text{Al}_2\text{O}_3\cdot 2\text{SiO}_2$ single phase zone. It is found that $\text{CaO}\cdot 2\text{Ce}_2\text{O}_3\cdot 3\text{SiO}_2$ is a favorable stable phase of RE elements according to the phase of the system. The synthesis range of $\text{CaO}\cdot 2\text{Ce}_2\text{O}_3\cdot 3\text{SiO}_2$ is quite wide and is greatly affected by temperature and slag composition, which indicates that a variety of components can be formed in the quaternary system. Therefore, according to the phase diagram, rare earth elements can be enriched into the $\text{CaO}\cdot 2\text{Ce}_2\text{O}_3\cdot 3\text{SiO}_2$ phase by controlling the appropriate composition of the slag containing rare earth elements. The current research provides indispensable thermodynamic data for RE-containing phase equilibrium, which is very important for sustainable recovery of REEs from REEs-containing slag. Additionally, the shaded area has not involved in current research, as shown in Fig. 7.

Fig. 7 Phase diagram of $\text{SiO}_2\text{-Ce}_2\text{O}_3\text{-CaO-25wt.\% Al}_2\text{O}_3$ system



Conclusions

The thermodynamic information plays a significant role in the recovery and utilization of slag systems containing rare earth elements and also establishes a crucial theoretical basis for the development of REEs application industry. And it is also beneficial to the development and application of rare earth in iron and steel industry and ceramic industry. The main results of the phase equilibrium relationship of SiO₂-Ce₂O₃-CaO-25wt.% Al₂O₃ system phase diagram at 1773 K investigated in current research can be summarized as follows:

- (1) Seven phases were determined by the current research work. It consists of a single liquid region, three primary crystal regions (C₂AS, 2CaO·SiO₂, CaO·2Ce₂O₃·3SiO₂) and three three-phase coexistence regions (L + C₂AS + 2CaO·SiO₂, L + C₂AS + CaO·2Ce₂O₃·3SiO₂, L + CaO·2Ce₂O₃·3SiO₂ + CeAl₁₁O₁₈).
- (2) The liquid isotherms and the phase relationship of SiO₂-Ce₂O₃-CaO-25wt.% Al₂O₃ system related to the cerium-containing slag system are established. According to the phase diagram, rare earth elements could be enriched into the CaO·2Ce₂O₃·3SiO₂ phase as much as possible by controlling the appropriate composition of the slag containing rare earth elements. The phase equilibrium data can provide a basis for comprehensive utilization of cerium-rare earth slag and optimization of related thermodynamic database.

References

1. Mohammed AA, Leonard Z, Michael GP (2012) Economics of rare earth elements in ceramic capacitors. *Ceram Int* 38:6091–6098
2. Xu CH, Huang CZ, Ai X (2006) Toughening and strengthening of advanced ceramics with rare earth additives. *Ceram Int* 32:423–429
3. Sadeq MS, Morshidy HY (2019) Effect of mixed rare-earth ions on the structural and optical properties of some borate glasses. *Ceram Int* 45:18327–18332
4. Yuan ZX, Bai G, Wu CY, Zhang ZQ, Ye XJ (1992) Geological features and genesis of the Bayan Obo REE ore deposit. *Inner Mongolia China Appl Geochem* 7:429–442
5. Zhang B, Liu CJ, Li CL, Jiang MF (2014) A novel approach for recovery of rare earths and niobium from Bayan Obo tailings. *Miner Eng* 65:17–23
6. Jordens A, Cheng YP, Waters KE (2013) A review of the beneficiation of rare earth element bearing minerals. *Miner Eng* 41:97–114
7. Humphries M (2010) Rare earth element: the global supply chain. Congressional Research Service, Washington, DC
8. Xu T, Peng HQ (2009) Formation cause, composition analysis and comprehensive utilization of rare earth solid wastes. *J Rare earth* 27:1096
9. Tas AC, Akinc M (1994) Phase relations in the system Ce₂O₃-Ce₂Si₂O₇ in the temperature range 1150°C to 1970°C in reducing and inert atmospheres. *J Am Ceram Soc* 77:2953–2960
10. Zhao Z, Chen X, Glaser B, Yan B (2019) Experimental study on the thermodynamics of the CaO-SiO₂-Ce₂O₃ system at 1873 K. *Metall Mater Trans B* 50:395–406
11. Lan X, Gao JT, Du Y, Guo ZC (2020) Thermodynamics and crystallization kinetics of REEs in CaO-SiO₂-Ce₂O₃ system. *J Am Ceram Soc* 103:2845–2858

12. Lan X, Gao JT, Li Y, Guo ZC (2021) Thermodynamics and kinetics of REEs in CaO-SiO₂-CaF₂-Ce₂O₃ system: a theoretical basis toward sustainable utilization of REEs in REE-bearing slag. *Ceram Int* 47:6130–6138
13. Lan X, Gao JT, Li Y, Guo ZC (2021) Phase equilibria of CaO-SiO₂-CaF₂-P₂O₅-Ce₂O₃ system and formation mechanism of britholite. *Ceram Int* 47:11966–11972
14. Li DG, Bu Q, Lou T, Sui ZT (2004) Morphology of solidified slag for RE₂O₃-CaO-SiO₂-CaF₂-MgO-Al₂O₃ system. *J Iron Steel Res Int* 16:30–33
15. Ding YG, Wang JS, Wang G, Xue QG (2012) Innovative methodology for separating of rare earth and iron from Bayan Obo complex iron ore. *ISIJ Int* 52:1772–1777
16. Wu Y, Ren G, Ding D, Yang F, Pan S (2012) Energy levels of Ce³⁺ in Lu_{0.8}Sc_{0.2}BO₃ host: a comparison study between x-ray photoelectron spectroscopy and pure optical method. *IEEE Trans Nucl Sci* 59:2069–2073
17. Pidol L, Viana B, Kahn-Harari A, Galtayries A, Bessiere A, Dorenbos P (2004) Optical properties and energy levels of Ce³⁺ in lutetium pyrosilicate scintillator crystal. *J Appl Phys* 95:7731–7737
18. Li M, Zhang T, Wang W, Zhang H, Li R. Experimental study on thermodynamics of CaO-SiO₂-Ce₂O₃-5wt.% Al₂O₃ system at 1773 K. *TMS* (2022)209–223
19. Won K, Smith A, Zeininger G (2006) Thermodynamic methods for pressure relief system design parameters. *Fluid Phase Equilib* 241:41–50
20. Elwert T, Goldmann D, Schirmer T, Strauss K (2014) Affinity of rare earth elements to silico-phosphate phases in the system Al₂O₃-CaO-MgO-P₂O₅-SiO₂. *Chem Ing Tech* 86:840–847
21. Gao P, Han Y, Sun Y, Chen C (2012) Research on the reaction behavior of rare earth elements in reduction. *Powder Technol Appl IV* 454:268–272
22. Wang Z, Sun H, Zhang L, Zhu Q (2016) Phase equilibria in the TiO₂ rich part of the TiO₂-CaO-SiO₂-10wt% Al₂O₃ system at 1773 K and 1873 K. *J Alloy Compd* 671:137–143
23. Gran J, Wang Y, Sichen D (2011) Experimental determination of the liquidus in the high basicity region in the Al₂O₃ (30 mass%)-CaO-MgO-SiO₂ system. *Calphad* 35:249–254
24. Verein Deutscher Eisenhüttenleute (1995) *SLAG ATLAS 2nd Edition*[M]. Verlag Stahleisen GmbH, p 105